NeuroImage **13,** 577–588 (2001)
doi:10.1006/nimg.2000.0716, available online at http://www.idealibrary.com on IDEAL®

Anatomic and Functional Variability: The Effects of Filter Size in Group fMRI Data Analysis

Tonya White,*,† Daniel O'Leary,* Vincent Magnotta,* Stephan Arndt,*,†,‡ Michael Flaum,*,† and Nancy C. Andreasen*,†

*Mental Health Clinical Research Center, †Department of Psychiatry, and ‡College of Public Health, University of Iowa Hospital and Clinics, Iowa City, Iowa 52241

Received June 6, 2000

In the analysis of group fMRI scans, an optimal spatial filter should be large enough to accurately blend functionally homologous anatomic regions, yet small enough not to blur the functionally distinct regions. Hanning filters varying from 0.0 to 18.0 mm were evaluated in a group analysis of six healthy controls performing a simple finger-tapping paradigm. Test–retest reliability and Talairach-based measurements of the sensorimotor region were used to explore the optimal filter size. Two distinct regions of functional activation were noted in the sensorimotor cortex in group images ($n = 6$) at both time 1 and time 2. These regions merge once the filter size exceeds approximately 6.0 mm. The original hypothesis that these represented a motor and sensory activation was rejected on the basis of structural and functional variability. A discussion of the inherent difficulties in choosing an appropriate filter size is presented. © 2001 Academic Press

Key Words: **fMRI; group analysis; filter size; spatial resolution.**

INTRODUCTION

The physiologic blood flow changes that occur with neuronal brain activation during cognitive or sensorimotor tasks serve as the basis for signal changes detected with fMRI (Ogawa *et al.,* 1990). The hemodynamic response following neuronal activation has been shown to display a biphasic course elicited through both optical imaging (Hu *et al.,* 1997; Malonek and Grinvald, 1996) and fMRI (Menon and Goodyear, 1999). The initial phase encompasses hemoglobin deoxygenation associated with the localized cortical activity. This initial and transient cortical activation is difficult to measure even at field strengths of 4 T (Menon and Goodyear, 1999). The secondary phase involves a hemodynamic feedback mechanism that results in increased blood flow to both the activated cortex and the regional venous system. This increased oxygenation has a greater signal-to-noise ratio compared to the initial deoxygenation phase and thus can be measured at lower field strengths. The hyperoxygenation phase is the most commonly used in fMRI studies.

Whereas the spatial resolution of the initial deoxygenation phase has been reported to be as fine as 700 μm (Menon and Goodyear, 1999), the spatial resolution of the hyperoxygenation phase is less clear. Changes in blood oxygenation can be demonstrated in the capillaries of cortical regions, in the local venules that lie within millimeters, and in the larger veins that may lie over a centimeter away from the region of activation (Boxerman *et al.,* 1995; Menon *et al.,* 1998). The localized blood oxygen level-dependent (BOLD) signal is modulated via the vascular hemodynamics (Gati *et al.,* 1997). While techniques utilizing both spatial position and flow characteristics can assist in discriminating the cortical activation signals from those signals obtained from larger vessels (Frahm *et al.,* 1994; Menon *et al.,* 1998), this continues to present a potential source for error in localizing brain activation. Nevertheless, a spatial resolution of 1.1 mm has been reported with imaging of the visual cortex at 1.5 T (Engel *et al.,* 1997a).

Even when submillimeter spatial resolution is routinely attained, the analysis of group data is confounded by both the anatomic and the functional variability between individuals (Friston *et al.,* 1989; Raichle *et al.,* 1991; Steinmetz and Seitz, 1991). Structural variability, defined as the spatial separation of an identical anatomic brain region between individuals, can be considerable even after brains are normalized in stereotactic space. For example, using Talairach coordinates, the central sulcus has been shown to have a 15- to 20-mm maximum range of variability between individuals (Steinmetz *et al.,* 1990; Talairach and Tournoux, 1988). Functional variability refers to the variation in the location of function on a gross anatomical level (Friston *et al.,* 1989). More specifically, it is the variability in the magnitude, shape, and location of a signal, within or between individuals performing an

1053-8119/01 $35.00

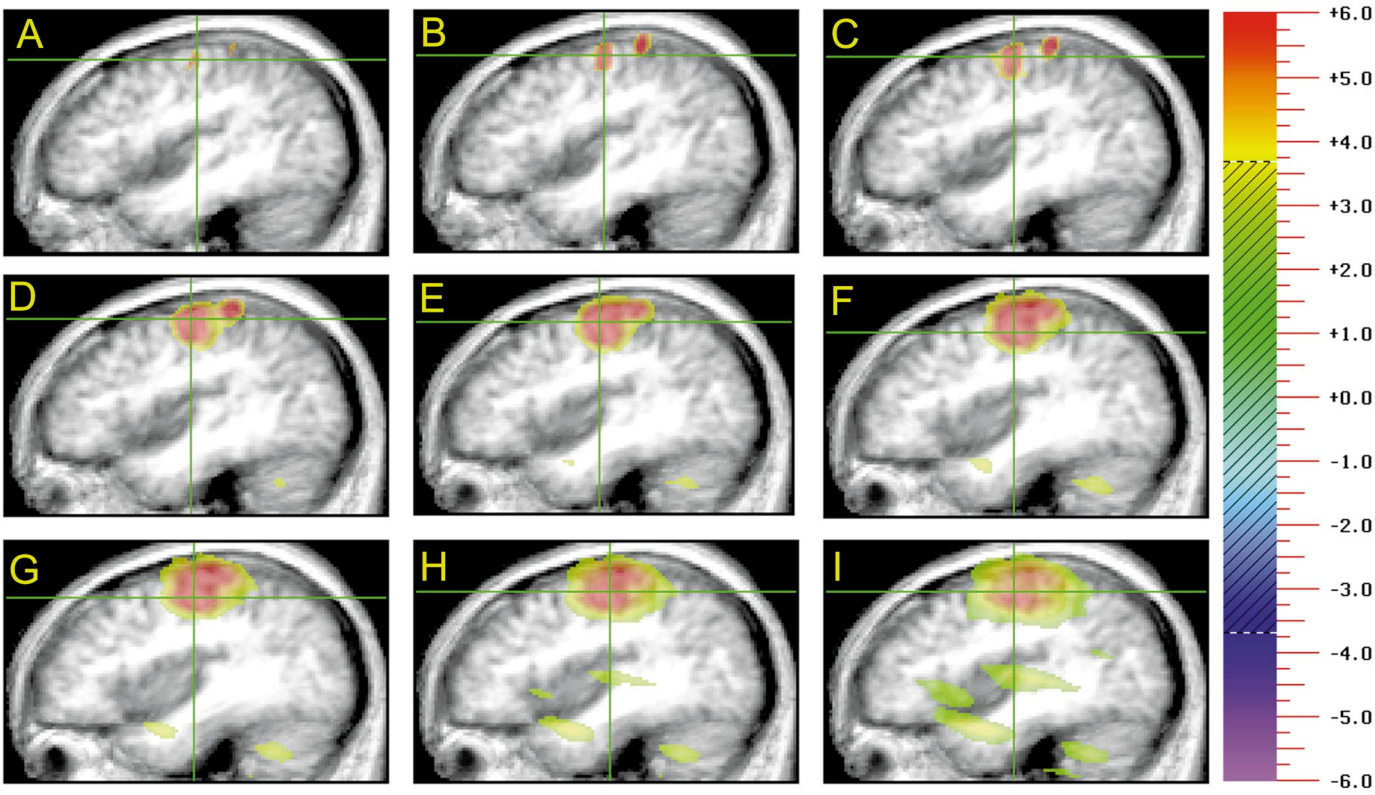

FIG. 1. Activation regions within the sensorimotor cortex at different Hanning filter sizes. The filter sizes are as follows: (A) 0, (B) 3.0, (C) 4.0, (D) 6.0, (E) 8.0, (F) 10.0, (G) 12.0, (H) 15.0, (I) 18.0 mm. Note the two distinct regions of activation with a filter size between 3.0 and 6.0 mm. The color scale is identical for Figs. 1–3 and has a threshold of $T = 3.67$.

identical task under controlled conditions. The functional brain architecture does not always correspond to a specific anatomic region across individuals (Steinmetz and Seitz, 1991). There exists both intra- and interindividual functional variability that depends on variables such differences in the strategy used to perform the task, the attention during the task, techniques used to perform the task, and cognitive factors influencing the task.

During a group analysis, this intersubject anatomic and functional variability creates both a signal reduction and a blurring of individual distinctions as coordinate systems are translated and coregistered (Cohen and Bookheimer, 1994; Raichle *et al.*, 1991; Steinmetz and Seitz, 1991). Single-subject designs preserve the anatomic and functional variability; however, group studies can be used to examine between-group differences between healthy volunteers and individuals suffering from specific illnesses that affect cognitive processes (e.g., schizophrenia). Group analyses are also used to determine the variance introduced by individual differences in cognitive strategies during complex tasks.

Two different fMRI group analysis techniques have evolved from previous work with positron emission tomography and single-photon emission computed tomography (Andreasen *et al.*, 1992b; Evans *et al.*, 1991; Fox, 1991; Fox *et al.*, 1985; Friston *et al.*, 1991; Mazziotta *et al.*, 1991; Worsley *et al.*, 1992). One technique, known as the "region of interest" or ROI approach, localizes specific brain regions either by tracing the ROI on a coregistered MRI scan or by applying a neuroanatomical template to the image (Bohm *et al.*, 1983; Evans *et al.*, 1991; Fox *et al.*, 1985; Friston *et al.*, 1989). An alternative ROI approach is to analyze individual statistical maps, define ROIs as functional activations at homologue anatomical locations, and then combine the results in a group (Crosson *et al.*, 1994; Fox and Raichle, 1984). The ROI approach is utilized when investigators have an a priori hypothesis regarding activation within a specific brain region and the statistical analysis evaluates the ROI between groups (Andreasen *et al.*, 1992b; Fox, 1991).

The second technique is termed a "function of interest" (FOI) approach and is well suited to exploratory studies mapping circuitry that is not yet well delineated (Arndt *et al.*, 1995). The most widely accepted FOI statistical approach is to transform the individual image data to a stereotaxic (e.g., Talairach and Tournoux, 1988) coordinate system and then group the images and make statistical inferences from the group differences (Fox *et al.*, 1985; Friston *et al.*, 1989; Maz-

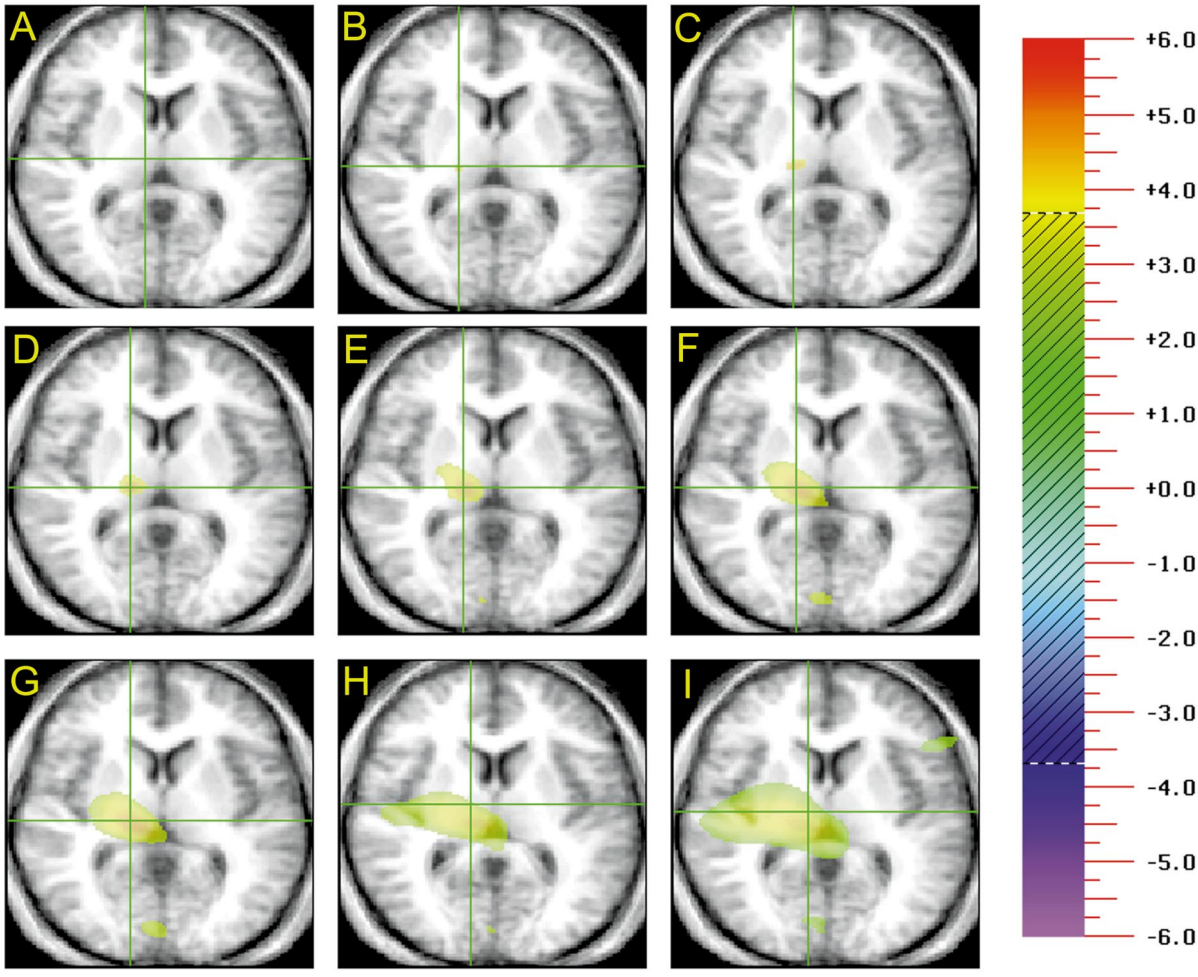

FIG. 2. Activation regions in the thalamus at different Hanning filter sizes. The filter sizes are as follows: (A) 0, (B) 3.0, (C) 4.0, (D) 6.0, (E) 8.0, (F) 10.0, (G) 12.0, (H) 15.0, (I) 18.0 mm. Note the blending of the thalamic activation with contralateral brain regions with a filter size greater than 8.0 mm. The color scale is identical for Figs. 1–3 and has a threshold of $T = 3.67$.

ziotta *et al.*, 1991; Worsley *et al.*, 1992). The majority of fMRI software packages currently available convolve the image volume with a spatial filter prior to the group analysis (Gold *et al.*, 1998). The spatial smoothing increases the signal-to-noise ratio and provides a filter-size-dependent merging of discrete activations (Lowe and Sorenson, 1997; Poline and Mazoyer, 1991, 1994). This filtering increases the probability that areas of activation will overlap during the coregistration of the group images, although the spatial resolution decreases inversely with increasing filter sizes (Mazziotta *et al.*, 1981). Utilizing a larger filter size is more likely to blend functionally discrete activations and shift the activation's center of mass. Thus, the goal is to utilize a filter that spreads the activation regions sufficiently to allow for an overlap of homologous activation sites during coregistration of group images, while preserving spatial resolution.

This study is an empirical examination of the effects of filter size on activation patterns using a very simple alternating right/left finger-tapping paradigm. The individual anatomic variability is measured and compared with the filter-dependent brain activation regions. A test–retest sequence is implemented to assess image acquisition and processing-dependent variability (i.e., head placement and movement, scanner instability, and image registration). The functional variability is controlled by utilizing a simple motor task with a well-defined pathway (Colebatch *et al.*, 1991; Ono *et al.*, 1990; Penfield and Boldrey, 1937; Roland *et al.*, 1980; Roland and Zilles, 1996).

METHODS

The subjects consisted of six healthy right-handed individuals, five males and one female, ranging in age from 19 to 41 years; mean age was 25.2 (SD 8.23) years. Each participant was screened to rule out general medical or psychiatric disorders. Informed consent was obtained from all subjects. A high-resolution structural

MRI scan was acquired to determine anatomic variability and to serve as a template for the functional images. Two fMRI scans were obtained approximately 3 weeks apart. The activation task consisted of repeated finger–thumb opposition at a high rate. The subjects alternated between their right and left hand in an "ABAB . . ." or "boxcar" design (A, right finger-tapping; B, left finger-tapping). The total AB cycle length was 40 s (20 s with each hand) and each cycle was repeated 12 times for a total of 480 s.

MR Data Acquisition

The high-resolution MR images were obtained on a 1.5-T GE Signa scanner. The T1-weighted images were acquired using a spoiled grass sequence obtained with the following parameters: 1.5-mm coronal slices, 40° flip angle, TR 24 ms, TE 5 ms, NEX 2, FOV 26 cm, and 256 × 192 matrix. Acquisition of the fMRI data was performed on a 1.5-T Siemens Magnetom scanner. The BOLD technique (Ogawa *et al.*, 1990) with an EPI paradigm was utilized with the following T2* parameters: TR 4 s; TE 40 ms; matrix size 128 × 128; FOV 24 × 24. Sixteen 6-mm slices were acquired with a 1-mm gap, covering the entire brain.

Postacquisition Image Processing

Following acquisition, the high-resolution MRI and fMRI data were transferred to the Image Processing Laboratory for processing on a Silicon Graphics workstation. Analyses were accomplished using the locally developed software package BRAINS (Brains Research: Analysis of Images, Networks, and Systems) (Andreasen *et al.*, 1992a), which has been modified to analyze fMRI data. The brain was reoriented along the anterior–posterior commisure (AC-PC) line and the interhemispheric fissure (Fox *et al.*, 1985; Friston *et al.*, 1989) and resampled at 1.0 mm^3. A bounding box of the brain and the AC-PC points were utilized to warp a spatially normalized Talairach grid (Talairach and Tournoux, 1988) onto the brains of each individual.

Each T2* image was realigned in two-dimensional space utilizing a three-parameter AIR 3.0 model (Woods *et al.*, 1998) to reduce the effects of movement during the fMRI scan. A cross-correlation method was used for analysis of individual data (Bandettini *et al.*, 1993) yielding correlation (r) maps. The analysis software also generated a mean time course image for each individual. The extraneous cranial tissue was removed from the mean time course image utilizing automated thresholding and erosion techniques. Utilizing a six-parameter AIR 3.0 algorithm (Woods *et al.*, 1998), each subject's mean time course image was registered to their corresponding spatially normalized T1-weighted image. Each image was assessed for quality of fit and all scans received a quality rating of good to excellent. A Fisher's r-to-Z transformation was done in order to make the r values resemble a normal distribution (Stuart and Ord, 1987).

The Talairach normalized functional scan for each individual was spatially smoothed with a Hanning filter, ranging from 0 to 18 mm full-width at half-maximum (FWHM), by increments of 1.0 mm. After filtering each individual image and coregistering the scans in Talairach space, a group analysis was performed and statistical parametric maps were generated using a modification of the Worsley technique (Worsley *et al.*, 1992). The Worsley analysis was used to determine the location of the activations within the group image. A λ matrix (Formula 3 in Worsley *et al.* (1992)) was generated to provide an estimate of resolution elements ("resels"). The λ matrix takes into account spatial autocorrelation caused by the local similarities of functional and spatial correlations produced by the filter. The number of resels will vary depending on the filter size, with larger filters having fewer resels. A significance threshold of $P < 0.05$ was applied for each filter size, corrected for the number of resels. Analyses were performed for both time 1 and time 2.

Monte Carlo Analysis

A Monte Carlo computer simulation was performed by placing random activations within the precentral gyrus in each of the six individuals. The random activations consisted of an amplified Gaussian distribution with a standard deviation ranging from 0 to 4 mm. The scaled Gaussian activation ranged from 0 to 10; however, since the focus of the modeling was to determine activation location rather than amplitude, the maximum amplitude of each simulation was normalized to the maximum value of the actual image. The normalization was performed after the simulations were filtered with a 4-mm Hanning filter and a group analysis was applied. The simulation was performed over 5000 iterations yielding one "best fit" output.

RESULTS

Different image results were obtained depending on the filter size utilized in the group analysis (see Figs. 1–3). Clusters of small distinct activations were observed in the sensorimotor region in the absence of a filter. These discrete activations merge into two distinct larger activations at a filter size of 3.0 mm. Once a filter size of 6.0 mm is surpassed, only one large activation in the sensorimotor cortex remains (Fig. 1). Filter sizes exceeding 12 mm only increase the size of the existing activations and cause a merging of activations at distant anatomic sites (e.g., the right sensorimotor activation merges with a left contralateral subcortical activation).

With respect to a finger-tapping task, expected activations were also present in the contralateral thala-

mus and ipsilateral cerebellum. A single thalamic activation appeared with a filter size of 3.0 mm and its volume increased relative to the filter size (Fig. 2). For smaller filters, the center of activation remained essentially fixed at both time 1 and time 2. Filter sizes greater than 8.0 mm, however, resulted in a shift in the activation's center of mass and a merging with functional activity at distant anatomic locations. In the absence of a filter, the cerebellum displayed a cluster of small discrete activations (Fig. 3). These discrete activations merged into a single activation with a 3.0-mm filter. Increasing the filter size beyond 3.0 mm only enlarged the volume of activation. This was true for both the thalamus and the cerebellum.

There are two clearly distinct activation regions in the sensorimotor cortex using a filter size of 4.0 mm (Fig. 1C). The region between these two activations can be visually represented in a one-dimensional topographical representation of the *T* scores. This is accomplished by defining a line in three-dimensional space that intersects the peak value for each of the two activations. When the *T* values along this line are plotted they provide a statistical parametric map of the activation topography in a one-dimensional graph (Fig. 4C). Applying this same technique to various filter sizes provides a visual representation of the merging of the two activations with increasing filter sizes (Fig. 4). The question arises as to which filter size provides the most accurate reflection of the underlying functional process?

The distance separating the two peak activations at a filter size of 4.0 mm was 18.9 mm (see Fig. 4C). Evaluating the anatomic location in Talairach coordinates of the central sulcus in 20 healthy subjects, Steinmetz *et al.* demonstrated that upper range of variability to be between 15 and 20 mm (Steinmetz *et al.*, 1990). This variability also corresponds with the central sulcus variability described by Talairach and Tournoux in their gross dissection of 20 brains (Talairach and Tournoux, 1988). The maximum range of central sulcus variability approached 20 mm in our 6 subjects and was 14.1 mm along the topographical line connecting the two activations. Thus, the 18.9-mm distance between the two peaks approaches the maximum possible distance attributable to anatomic variability. It thus became imperative to match the underlying anatomy with the activation regions in each individual.

Each of the six individual fMRI scans was filtered with a 4.0-mm Hanning filter and coregistered to Talairach space. Utilizing the same one-dimensional topographic representation as the group image, the statistical parametric map for each individual was plotted along the same predefined line (Fig. 5). This provides a visual representation of the individual activation topography that contributes to the two group activations (see Fig. 6A). Next, the central sulci and postcentral sulci were identified in Talairach space utilizing the high-resolution structural MR scans. The point at which the central and postcentral sulci intersect the topographical line was plotted. Figure 5 displays the six individual line plots with the precentral and postcentral sulci identified.

One of the individuals had an unequivocal isolated postcentral activation (Fig. 5A). In fact, this pronounced activation was predominantly posterior to the postcentral sulcus. Another individual had a predominant precentral activation (Fig. 5B). One individual had pronounced postcentral activation and a smaller precentral activation (Fig. 5C). The remaining three individuals displayed smaller, but consistent activations directly overlaying the central and postcentral sulci (Figs. 5D–5F). These latter three activations are smaller in amplitude and are less distinguishable from background noise. However, these activations contribute to the *T* test performed to yield the two activation regions in the group image (see Figs. 6A and 6B).

When the axes of the topographical *Z* maps are translated such that the central sulci of each individual corresponds with 0.0 mm, there is a distinct blurring of the two activation peaks (Figs. 6C and 6D). The individual anatomic and functional variability blurs the distinction between the two activations. A *T* test performed using the translated statistical parametric maps for each individual results in one large activation with the greatest magnitude directly over the location of the central sulcus (Fig. 6D). This topographical *T* map closely resembles the group analysis filtered at 10.0 mm (Fig. 4F).

A computer model was generated to determine if structural variability alone could account for the two activations. Activations of random magnitude and amplitude were generated and randomly placed in the precentral gyrus of each of the six individuals. The center of mass for the computer-generated activations did not exceed 5.0 mm caudal to the central sulcus. A 4.0-mm Hanning filter was applied to each activation and a Worsley analysis was performed on the randomly distributed activations. After 5000 iterations, the model was unable to approximate the pattern of two distinct activations. Thus, it was not structural variability alone that accounted for the presence of two distinct activations, but rather the combination of functional and structural heterogeneity between individuals.

DISCUSSION

With the ability to detect brain activity at spatial resolutions approaching 1.0 mm (at 1.5 T), fMRI is a powerful tool in the functional assessment of the brain. Single-subject designs preserve both functional and spatial resolution and are valuable in addressing specific scientific questions (Cohen and Bookheimer, 1994). Group studies, however, are an important strat-

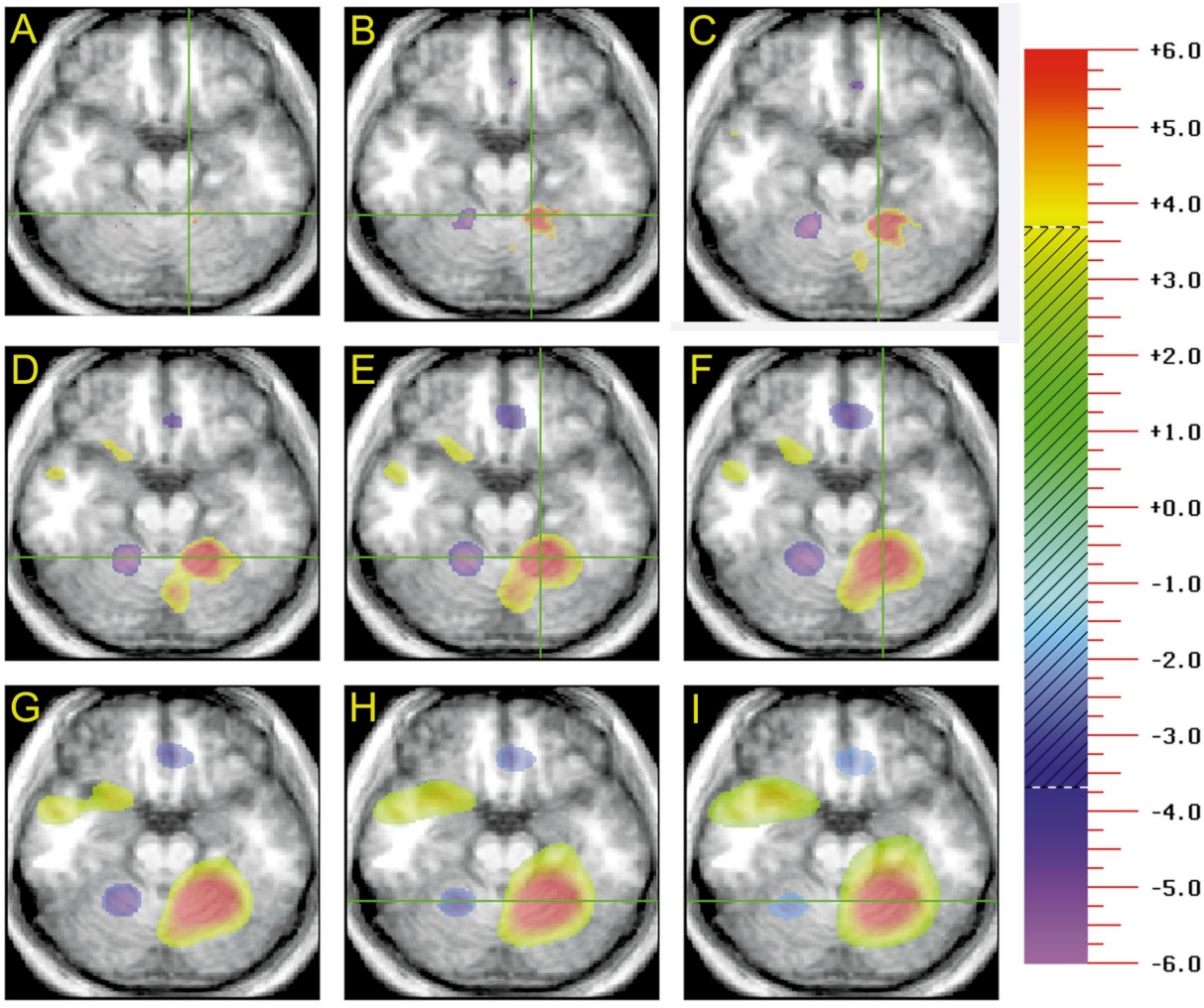

FIG. 3. Activation regions in the thalamus at different Hanning filter sizes. The filter sizes are as follows: (A) 0, (B) 3.0, (C) 4.0, (D) 6.0, (E) 8.0, (F) 10.0, (G) 12.0, (H) 15.0, (I) 18.0 mm. Note that the single activation present with a 3-mm filter only increases in volume with increasing filter sizes. The color scale is identical for Figs. 1–3 and has a threshold of $T = 3.67$.

egy for obtaining generalized answers to a number of scientific questions. Techniques are needed to pool individuals in the formation of groups. However, the validity of those techniques must also be examined.

Spatial filters are commonly utilized during the post-processing of fMRI both to enhance the signal detection and to smooth and distribute the image prior to the group analysis (Kruggel *et al.*, 1999; Lowe and Sorenson, 1997; Poline and Mazoyer, 1994). Although the absence of a filter will preserve the individual spatial resolution, areas of correlation that are functionally homologous, yet anatomically separate may fail to overlap and thus fail to demonstrate significance in a group FOI analysis. The use of an excessively large filter size, however, will limit the spatial resolution and may cause a blurring of unrelated functional regions (Mazziotta *et al.*, 1981). Thus an optimal filter should be large enough to provide an overlap of functionally homologous activations, while small enough to preserve the anatomic localization and functionally distinct regions.

As two needle sticks are necessary to evaluate the spatial resolution of detecting two distinct pricks on the skin, so too can a simple task involving a well-defined anatomical pathway be utilized to determine filter parameters to optimize imaging resolution. An a priori supposition was that functional variability would be significantly reduced with a simple motor paradigm such as alternating finger-tapping.

Two very distinct regions of activation emerge within the sensorimotor cortex in the group image at lower filter sizes (Figs. 1A–1C). These blend into one primary activation as the filter size exceeds 6.0 mm (Figs. 1D–1I). The original hypothesis was that these represented two distinct activations, one anterior and the other posterior to the central sulcus. Previous anatomic work, dating back to the early work of Penfield and Boldrey (1937), has demonstrated specific neuronal

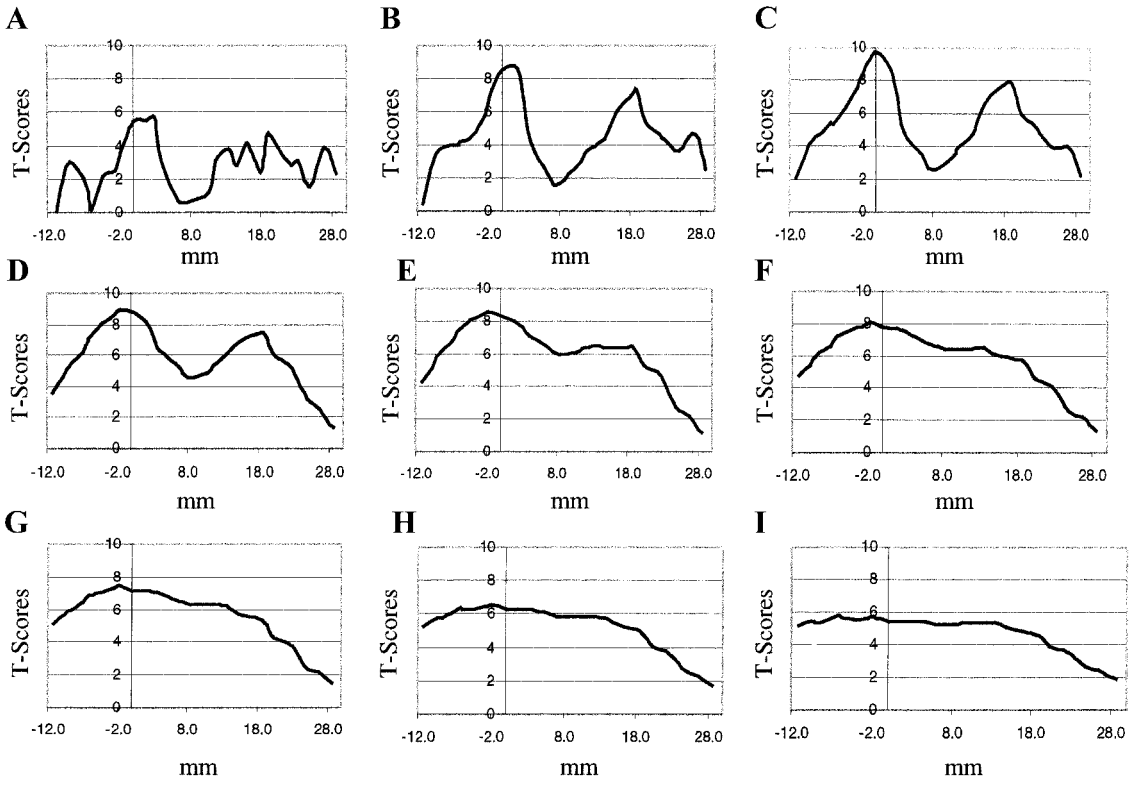

FIG. 4. A one-dimensional topographic representation of the region between the two activations at different filter sizes. This was generated by tracing the *T* values along a line connecting the two points of peak activation using the 4.0-mm-filtered group data (C). The Talairach coordinates for the anterior activation are (42, −17, 52), and the coordinates for the posterior activation are (45, −35, 57). This same topographic line is utilized to display the region between the activations at different filter sizes: (A) 0, (B) 3.0, (C) 4.0, (D) 6.0, (E) 8.0, (F) 10.0, (G) 12.0, (H) 15.0, (I) 18.0 mm.

pathways for a simple motor task such as finger-tapping. The efferent corticospinal tract originates primarily in the primary motor cortex, which lies anterior to the central sulcus and descends through the internal capsule. Sensory information decussates at the level of the spinal column prior to coursing up the spinothalamic tract to the ventral posteriolateral thalamic nuclei (VPL) (Jones, 1985; Macchi and Jones, 1997). Efferent projections from the VPL terminate in the postcentral gyrus (Parent, 1996).

However, evidence is also emerging to suggest that sensory/motor pathways are not purely dichotomous. Corticospinal fibers have been reported to arise from the premotor area (area 6), postcentral gyrus (areas 1, 2, 3a, 3b), and adjacent parietal cortex (area 5) (Parent, 1996). Cortical mapping of the sensorimotor region with subdural grid electrodes has demonstrated postcentral responses to motor movements of the fingers in approximately one-fourth of individuals (Nii *et al.*, 1996; Penfield and Boldrey, 1937). Precentral sensory activity has also been reported, although the literature is mixed. Several reports have shown that a precentral response to sensory information is a rare event (Penfield and Boldrey, 1937; Puce *et al.*, 1995; Woolsey *et al.*, 1979), while a recent report describes precentral activation to sensory stimulation in 74% of individuals (Nii *et al.*, 1996).

Numerous fMRI studies have evaluated the motor region, often comparing the location with direct electrophysiologic measures of the elegant cortex (Toga *et al.*, 1995). These studies demonstrate both pre- and postcentral activation with the motor function predominantly in the precentral sulcal region (Boecker *et al.*, 1994; Puce *et al.*, 1995; Toga *et al.*, 1995). Electrophysiologic measures are more likely to show activation regions corresponding to the crest of the gyral regions, whereas fMRI activations are often present directly within the central sulci (Toga *et al.*, 1995). This may be a result of activation signals detected by venous flow within central sulcus (Haacke *et al.*, 1994; Shimizu *et al.*, 1997; Yousry *et al.*, 1996). Additionally, intersubject differences in rate and force of movement, movement strategies, and previous experience (i.e., a professional typist) can also influence the functional patterns. A group analysis of subjects, however, may reveal that the motor/sensory dichotomy becomes the statistically predominant functional process, thus resulting in two distinct activations.

The physiologic explanation for the presence of two distinct activations, as described above, is one of sev-

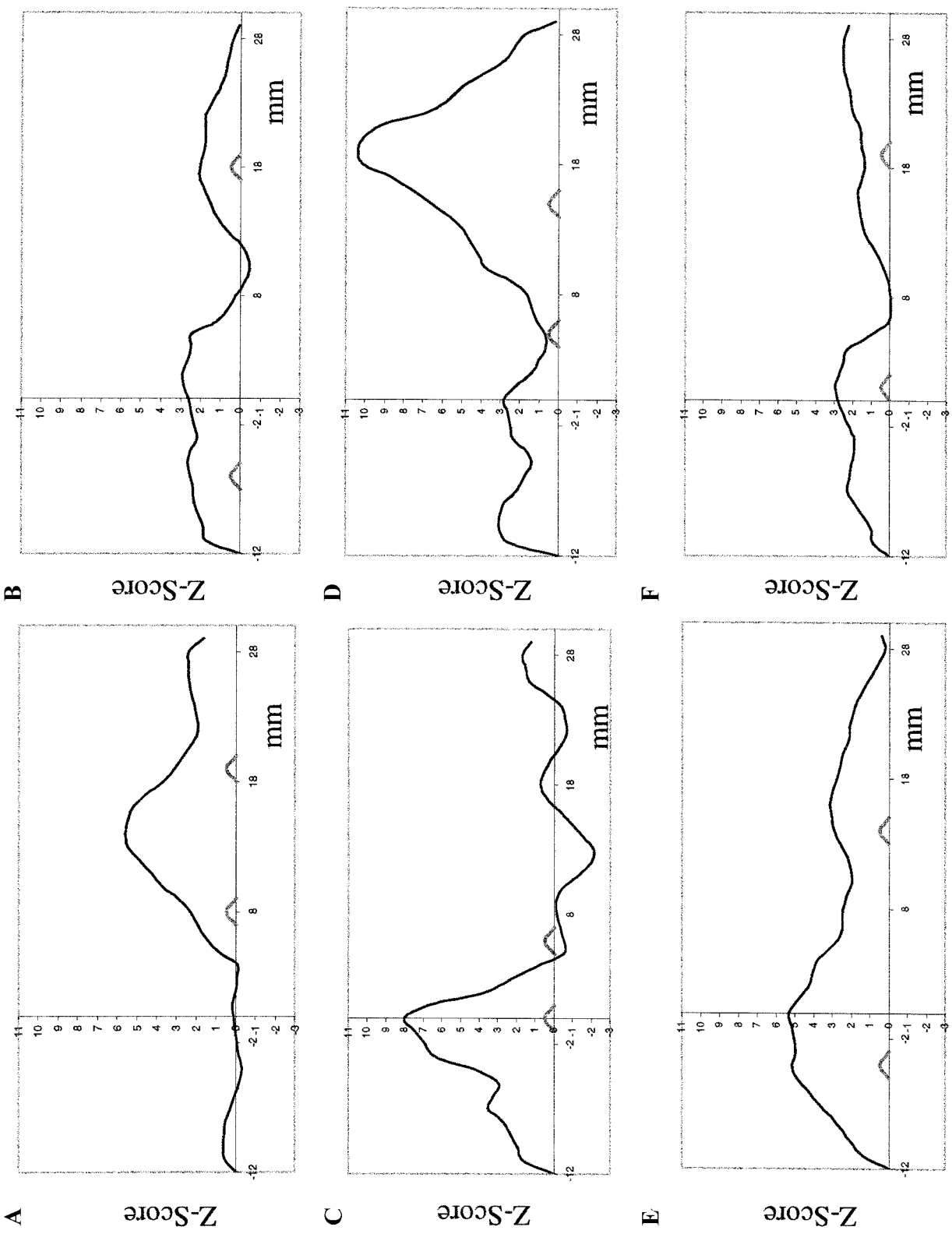

FIG. 5. The *Z* scores for each individual are plotted at the same Talairach-defined locations along the line between the two activations in the group analysis. This provides a one-dimensional topographic representation of each individual's contribution to the two activation regions. Also seen are the locations where this line intersects the central suclus (left hash mark) and postcentral sulcus (right hash mark).

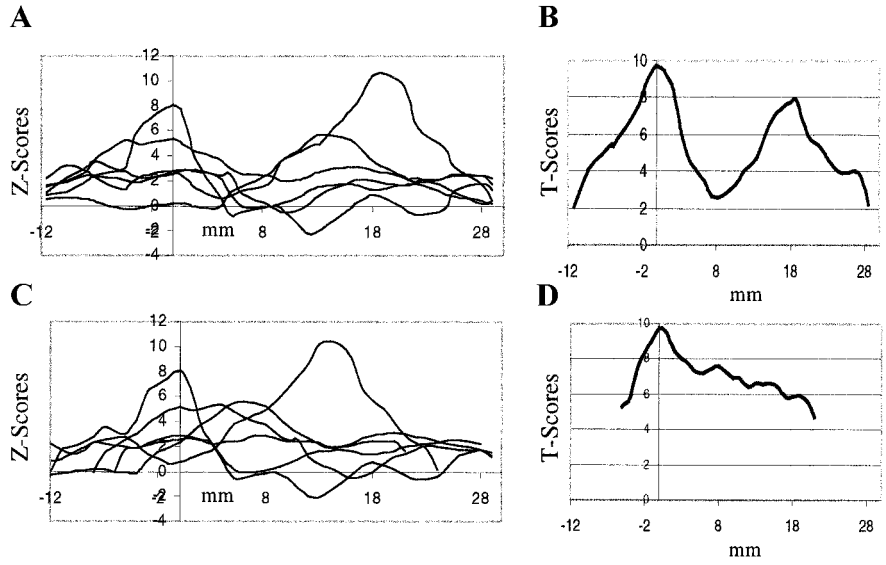

FIG. 6. (A) The one-dimensional statistical parametric maps for each individual (shown in Fig. 5) are plotted together at the same Talairach-defined locations along the line between the two activations. The two activation sites are readily identifiable in this representation. It can be seen that the large activation region, posterior to the postcentral sulcus (Fig. 3D) appears to drive the posterior activation. The Talairach coordinates for the anterior activation are (42, −17, 52) and for the posterior activation are (45, −35, 57). (B) A *T* map of the individual activations shown in (A) clearly demonstrates the presence of two activation regions. (C) The axes of each individual are translated so that the central sulcus is aligned at 0. (D) A *T* test performed on the translated data of (C) demonstrates that the two activation regions have merged.

eral. Alternate mechanisms that could result in two distinct activations include: (i) the variation in brain morphology during coregistration and overlap of individual images (Cohen and Bookheimer, 1994), (ii) differences in gradient design and unwarping algorithms between the high-resolution MRI scanner and the scanner used to obtain the fMRI data, (iii) venous or flow artifacts in the vicinity of larger vessels (Frahm *et al.*, 1994; Shimizu *et al.*, 1997; Yousry *et al.*, 1996), (iv) head movement and physiologic artifacts (Kruggel *et al.*, 1999), (v) statistical techniques (Arndt *et al.*, 1995), (vi) scanner instability (Kruggel *et al.*, 1999), (vii) functional hetrogeneity (Friston *et al.*, 1989; Steinmetz and Seitz, 1991), (viii) intrasubject coregistration, and (ix) noise.

As the dual activations were present at both time 1 and time 2, the probability of generating two activations related to scanner instability, coregistration of images, movement, noise, or image-processing artifacts was significantly diminished. The structural, vascular, and functional heterogeneity between brains, however, remained as a potential source of variability over both time 1 and time 2. The distance separating the two activations was 18.9 mm, which is close to the maximum variability of previous reports of the central sulcus (Steinmetz *et al.*, 1990; Talairach and Tournoux, 1988). Computer modeling functional activations anterior to the central sulcus demonstrated that the two activations were not attributed to structural variability alone. However, when individual coregistered MRI and fMRI data were examined, it became clear that both anatomic and functional variability accounted for the presence of the two distinct activations.

Whereas spatially smoothing the sensorimotor cortex with an 8.0- to 10.0-mm FWHM filter was sufficient to account for the structural and functional variability of this region, it was too large for other regions. Increasing the filter size beyond 4.0 mm in the thalamic and cerebellar regions serves only to increase the activation volume and thus reduce resolution (Figs. 2 and 3). Since the anterior and posterior commissures are utilized as reference points in coregistering brains to Talairach coordinates (Talairach and Tournoux, 1988), less anatomic variability would be expected for structures neighboring these reference points (Mazziotta *et al.*, 1995). For example, the range of anatomic variability of the lateral border of the thalamus in our subjects was between 0.7 and 2.1 mm. Thus, regions with less intersubject variability warrant a smaller filter size, e.g., between 3.0 and 5.0 mm preserved structural resolution in this study.

It is not realistic for one filter size to preserve the structural resolution and prevent the overlap of distinct activations within all brain regions. When the shape of the activation region is known, morphologic filters can optimize the signal-to-noise ratio (Poline and Mazoyer, 1991). However, the shape of the activation is often unknown, especially when utilizing an FOI approach. When specific anatomic connections are known (e.g., the cortical–cerebellar–thalamic circuits

utilized in the motor system) several images derived using different filter sizes dependent on the brain region can be utilized, for example, applying a 3.0-mm filter for the subcortical and thalamic regions and a 10.0-mm filter for the cortical regions, as evidenced in this study. The statistical implications of varying filter size across brain regions is beyond the scope of this paper; however, it has been described by Worsley *et al.* (1996).

As an alternative to variable filters, smaller filter sizes (i.e., 3–5 mm) will preserve the subcortical resolution while neighboring activations in the cortical regions should not be considered distinct until the individual contributions are evaluated. Finally, the use of a multifiltering technique (Poline, 1994; Worsley *et al.*, 1996) applied to a group analysis or a filter size that is related to the distance from the AC-PC line are possibilities that require further exploration.

There are several limitations to the present study. The subject population was quite small and thus individual differences are more likely to influence the group analysis. A larger subject pool would increase the variability of the activations within the sensorimotor region and likely obscure the two activation regions. Although a direct comparison of an ROI and an FOI approach was not performed, an ROI approach that separated the pre- and postcentral sulci may dichotomize two functionally homologous units. A study utilizing an ROI approach to determine the contribution of the tactile component of the finger-tapping paradigm found no significant difference whether or not the finger and thumb made contact (Jansma *et al.*, 1998). Proprioception may contribute to the sensory activation patterns and the instruction not to touch may also invoke a sensory signal similar to that seen with phantom limbs (Ersland *et al.*, 1996).

It is possible to generate a mathematical algorithm to choose a filter size given a specific anatomic variability. Two simultaneously imaged activations can be discriminated when the distance between them is at least one point-spread function at its half-maximum (FWHM). However, such an algorithm would require the inclusion of the functional variability of the region of interest, which is usually not known. This becomes even more problematic when activations occur in brain regions that are not as anatomically delineated as the sensorimotor cortex, i.e., activations in the frontal or temporal lobes. Furthermore, greater interindividual functional variability may be present in these regions. Baseline functional maps that trace out activation patterns for an individual prior to an actual study or probabilistic atlases that blend both structure and function may prove beneficial in addressing these questions (Mazziotta *et al.*, 1995). Finally, in order to capture the enhanced spatial resolution that accompanies advancements in fMRI technology, evolving methodologies, such as those that reduce structural heterogeneity (Engel *et al.*, 1997b; Van Essen and Drury, 1997; Zeineh *et al.*, 2000), may eventually reduce the necessity of spatial smoothing.

It is clear that the choice of filter size used in group analyses is not straightforward. The choice of filter size can dramatically alter the final results presented. Smaller filter sizes may give misleading results without exploration of the underlying anatomy. Larger filter sizes are more likely to blend functionally distinct regions and result in a loss of anatomic specificity. An ROI approach may offer more precise anatomic localization of the activations; however, anatomic location and function may not always coincide. Using smaller filter sizes (e.g., 3.0 to 6.0 mm) provides the highest spatial resolution and is reasonable so long as attention is paid to the individual contributions of neighboring activations.

REFERENCES

Andreasen, N. C., Cohen, G., Harris, G., Cizadlo, T., Parkkinen, J., Rezai, K., and Swayze, V. W. d. 1992a. Image processing for the study of brain structure and function: Problems and programs. *J. Neuropsychiatry Clin. Neurosci.* **4:** 125–133.

Andreasen, N. C., Rezai, K., Alliger, R., Swayze, V. W. d., Flaum, M., Kirchner, P., Cohen, G., and O'Leary, D. S. 1992b. Hypofrontality in neuroleptic-naive patients and in patients with chronic schizophrenia. Assessment with xenon 133 single-photon emission computed tomography and the Tower of London. *Arch. Gen. Psychiatry* **49:** 943–958.

Arndt, S., Cizadlo, B., Andreasen, N., Zeien, G., Harris, M., O'Leary, D., Watkins, G., Ponto, L., and Hichwa, R. 1995. A comparison of approaches to the statistical analysis of $[^{15}O]H_2O$ PET cognitive activation studies. *J. Neuropsychiatry* **7:** 155–168.

Bandettini, P. A., Jesmanowicz, A., Wong, E. C., and Hyde, J. S. 1993. Processing strategies for time-course data sets in functional MRI of the human brain. *Magn. Reson. Med.* **30:** 161–173.

Boecker, H., Kleinschmidt, A., Requardt, M., Hanicke, W., Merboldt, K. D., and Frahm, J. 1994. Functional cooperativity of human cortical motor areas during self-paced simple finger movements. A high-resolution MRI study. *Brain* **117:** 1231–1239.

Bohm, C., Greitz, T., Kingsley, D., Berggren, B. M., and Olsson, L. 1983. Adjustable computerized stereotaxic brain atlas for transmission and emission tomography. *Am. J. Neuroradiol.* **4:** 731–733.

Boxerman, J. L., Bandettini, P. A., Kwong, K. K., Baker, J. R., Davis, T. L., Rosen, B. R., and Weisskoff, R. M. 1995. The intravascular contribution to fMRI signal change: Monte Carlo modeling and diffusion-weighted studies in vivo. *Magn. Reson. Med.* **34:** 4–10.

Cohen, M. S., and Bookheimer, S. Y. 1994. Localization of brain function using magnetic resonance imaging. *Trends Neurosci.* **17:** 268–277.

Colebatch, J. G., Deiber, M. P., Passingham, R. E., Friston, K. J., and Frackowiak, R. S. 1991. Regional cerebral blood flow during voluntary arm and hand movements in human subjects. *J. Neurophysiol.* **65:** 1392–1401.

Crosson, B., Williamson, D. J., Shukla, S. S., Honeyman, J. C., and Nadeau, S. E. 1994. A technique to localize activation in the human brain with technetium-99m-HMPAO SPECT: A validation study using visual stimulation. *J. Nucl. Med.* **35:** 755–763.

Engel, S., Zhang, X., and Wandell, B. 1997a. Colour tuning in human visual cortex measured with functional magnetic resonance imaging. *Nature* **388:** 68–71.

Engel, S. A., Glover, G. H., and Wandell, B. A. 1997b. Retinotopic organization in human visual cortex and the spatial precision of functional MRI. *Cereb. Cortex* **7:** 181–192.

Ersland, L., Rosen, G., Lundervold, A., Smievoll, A. I., Tillung, T., Sundberg, H., and Hugdahl, K. 1996. Phantom limb imaginary fingertapping causes primary motor cortex activation: An fMRI study. *NeuroReport* **8:** 207–210.

Evans, A. C., Marrett, S., Torrescorzo, J., Ku, S., and Collins, L. 1991. MRI–PET correlation in three dimensions using a volume-of-interest (VOI) atlas. *J. Cereb. Blood Flow Metab.* **11:** A69–78.

Fox, P. 1991. Physiological ROI definition by image subtraction. *J. Cereb. Blood Flow Metab.* **11:** A79–A82.

Fox, P. T., Perlmutter, J. S., and Raichle, M. E. 1985. A stereotactic method of anatomical localization for positron emission tomography. *J. Comput. Assisted Tomogr.* **9:** 141–153.

Fox, P. T., and Raichle, M. E. 1984. Stimulus rate dependence of regional cerebral blood flow in human striate cortex, demonstrated by positron emission tomography. *J. Neurophysiol.* **51:** 1109–1120.

Frahm, J., Merboldt, K.-D., Hänicke, W., Kleinschmidt, A., and Boecker, H. 1994. Brain or vein—Oxygenation or flow? On signal psychology in function MRI of human brain activation. *NMR Biomed.* **7:** 45–53.

Friston, K. J., Frith, C. D., Liddle, P. F., and Frackowiak, R. S. 1991. Comparing functional (PET) images: The assessment of significant change. *J. Cereb. Blood Flow Metab.* **11:** 690–699.

Friston, K. J., Passingham, R. E., Nutt, J. G., Heather, J. D., Sawle, G. V., and Frackowiak, R. S. 1989. Localisation in PET images: Direct fitting of the intercommissural (AC-PC) line. *J. Cereb. Blood Flow Metab.* **9:** 690–695.

Gati, J. S., Menon, R. S., Ugurbil, K., and Rutt, B. K. 1997. Experimental determination of the BOLD field strength dependence in vessels and tissue. *Magn. Reson. Med.* **38:** 296–302.

Gold, S., Christian, B., Arndt, S., Zeien, G., Cizadlo, T., Johnson, D. L., Flaum, M., and Andreasen, N. C. 1998. Functional MRI statistical software packages: A comparative analysis. *Hum. Brain Mapp.* **6:** 73–84.

Haacke, E. M., Hopkins, A., Lai, S., Buckley, P., Friedman, L., Meltzer, H., Hedera, P., Friedland, R., Klein, S., Thompson, L., *et al.* 1994. 2D and 3D high resolution gradient echo functional imaging of the brain: Venous contributions to signal in motor cortex studies. *NMR Biomed.* **7:** 54–62. [Published erratum appears in *NMR Biomed.*, 1994, **7:** 374]

Hu, X., Le, T. H., and Ugurbil, K. 1997. Evaluation of the early response in fMRI in individual subjects using short stimulus duration. *Magn. Reson. Med.* **37:** 877–884.

Jansma, J. M., Ramsey, N. F., and Kahn, R. S. 1998. Tactile stimulation during finger opposition does not contribute to 3D fMRI brain activity pattern. *NeuroReport* **9:** 501–505.

Jones, E. G. 1985. *The Thalamus.* Plenum, New York.

Kruggel, F., von Cramon, D. Y., and Descombes, X. 1999. Comparison of filtering methods for fMRI datasets. *NeuroImage* **10:** 530–543, doi:10.1006/nimg.1999.0490.

Lowe, M. J., and Sorenson, J. A. 1997. Spatially filtering functional magnetic resonance imaging data. *Magn. Reson. Med.* **37:** 723–729.

Macchi, G., and Jones, E. G. 1997. Toward an agreement on terminology and subnuclear divisions of the motor thalamus. *J. Neurosurg.* **86:** 670–685.

Malonek, D., and Grinvald, A. 1996. Interactions between electrical activity and cortical microcirculation revealed by imaging spectroscopy: Implications for functional brain mapping. *Science* **272:** 551–554.

Mazziotta, J. C., Pelizzari, C. C., Chen, G. T., Bookstein, F. L., and Valentino, D. 1991. Region of interest issues: The relationship between structure and function in the brain. *J. Cereb. Blood Flow Metab.* **11:** A51–56.

Mazziotta, J. C., Phelps, M. E., Plummer, D., and Kuhl, D. E. 1981. Quantitation in positron emission computed tomography. 5. Physical–anatomical effects. *J. Comput. Assisted Tomogr.* **5:** 734–743.

Mazziotta, J. C., Toga, A. W., Evans, A., Fox, P., and Lancaster, J. 1995. A probabilistic atlas of the human brain: Theory and rationale for its development. The International Consortium for Brain Mapping (ICBM). *NeuroImage* **2:** 89–101, doi:10.1006/nimg.1995.1012.

Menon, R. S., Gati, J. S., Goodyear, B. G., Luknowsky, D. C., and Thomas, C. G. 1998. Spatial and temporal resolution of functional magnetic resonance imaging. *Biochem. Cell. Biol.* **76:** 560–571.

Menon, R. S., and Goodyear, B. G. 1999. Submillimeter functional localization in human striate cortex using BOLD contrast at 4 Tesla: Implications for the vascular point-spread function. *Magn. Reson. Med.* **41:** 230–235.

Nii, Y., Uematsu, S., Lesser, R. P., and Gordon, B. 1996. Does the central sulcus divide motor and sensory functions? Cortical mapping of human hand areas as revealed by electrical stimulation through subdural grid electrodes. *Neurology* **46:** 360–367.

Ogawa, S., Lee, T. M., Nayak, A. S., and Glynn, P. 1990. Oxygenation-sensitive contrast in magnetic resonance image of rodent brain at high magnetic fields. *Magn. Reson. Med.* **14:** 68–78.

Ono, M., Kubik, S., and Abernathy, C. D. 1990. *Atlas of Cerebral Sulci.* Thieme, Stuttgart.

Parent, A. 1996. *Carpenter's Human Neuroanatomy.* Williams & Wilkins, Baltimore.

Penfield, W., and Boldrey, E. 1937. Somatic motor and sensory representation in the cerebral cortex of man as studied by electrical stimulation. *Brain* **60:** 389–443.

Poline, J. B., and Mazoyer, B. M. 1991. Towards an individual analysis of brain activation PET studies: Optimal filtering of difference images. *J. Cereb. Blood Flow Metab.* **11**(Suppl. 2): S564.

Poline, J. B., and Mazoyer, B. M. 1994. Enhanced detection in brain activation maps using a multifiltering approach. *J. Cereb. Blood Flow Metab.* **14:** 639–642.

Puce, A., Constable, R. T., Luby, M. L., McCarthy, G., Nobre, A. C., Spencer, D. D., Gore, J. C., and Allison, T. 1995. Functional magnetic resonance imaging of sensory and motor cortex: Comparison with electrophysiological localization. *J. Neurosurg.* **83:** 262–270.

Raichle, M. E., Mintun, M. A., Shertz, L. D., Fusselman, M. J., and Miezen, F. 1991. The influence of anatomical variability on functional brain mapping with PET: A study of intrasubject versus intersubject averaging. *J. Cereb. Blood Flow Metab.* **11**(Suppl. 2): S364.

Roland, P. E., Larsen, B., Lassen, N. A., and Skinhoj, E. 1980. Supplementary motor area and other cortical areas in organization of voluntary movements in man. *J. Neurophysiol.* **43:** 118–136.

Roland, P. E., and Zilles, K. 1996. Functions and structures of the motor cortices in humans. *Curr. Opin. Neurobiol.* **6:** 773–781.

Shimizu, H., Nakasato, N., Mizoi, K., and Yoshimoto, T. 1997. Localizing the central sulcus by functional magnetic resonance imaging and magnetoencephalography. *Clin. Neurol. Neurosurg.* **99:** 235–238.

Steinmetz, H., Furst, G., and Freund, H. J. 1990. Variation of perisylvian and calcarine anatomic landmarks within stereotaxic proportional coordinates. *Am. J. Neuroradiol.* **11:** 1123–1130.

Steinmetz, H., and Seitz, R. J. 1991. Functional anatomy of language processing: Neuroimaging and the problem of individual variability. *Neuropsychologia* **29:** 1149–1161.

Stuart, A., and Ord, J. K. 1987. *Kendall's Advanced Theory of Statistics.* Oxford Univ. Press, London.

Talairach, J., and Tournoux, P. 1988. *Co-planar Stereotactic Atlas of the Human Brain: 3-Dimensional Proportional System: An Approach to Cerebral Imaging.* Thieme, Stuttgart.

Toga, A. W., Cannestra, A. F., and Black, K. L. 1995. The temporal/spacial evolution of optical signals in human cortex. *Cereb. Cortex* **5:** 561–565.

Van Essen, D. C., and Drury, H. A. 1997. Structural and functional analyses of human cerebral cortex using a surface-based atlas. *J. Neurosci.* **17:** 7079–7102.

Woods, R. P., Grafton, S. T., Holmes, C. J., Cherry, S. R., and Mazziotta, J. C. 1998. Automated image registration. I. General methods and intrasubject, intramodality validation. *J. Comput. Assisted Tomogr.* **22:** 139–152.

Woolsey, C. N., Erickson, T. C., and Gilson, W. E. 1979. Localization in somatic sensory and motor areas of human cerebral cortex as determined by direct recording of evoked potentials and electrical stimulation. *J. Neurosurg.* **51:** 476–506.

Worsley, K. J., Evans, A. C., Marrett, S., and Neelin, P. 1992. A three-dimensional statistical analysis for CBF activation studies in human brain. *J. Cereb. Blood Flow Metab.* **12:** 900–918.

Worsley, K. J., Marrett, S., Neelin, P., and Evans, A. C. 1996. Searching scale space for activation in PET images. *Hum. Brain Mapp.* **4:** 74–90.

Yousry, T. A., Schmid, U. D., Schmidt, D., Hagen, T., Jassoy, A., and Reiser, M. F. 1996. The central sulcal vein: A landmark for identification of the central sulcus using functional magnetic resonance imaging. *J. Neurosurg.* **85:** 608–617.

Zeineh, M. M., Engel, S. A., and Bookheimer, S. Y. 2000. Application of cortical unfolding techniques to functional MRI of the human hippocampal region. *NeuroImage* **11:** 668–683, doi:10.1006/nimg.2000.0561.